communications earth & environment

A Nature Portfolio journal

Article

https://doi.org/10.1038/s43247-025-02931-9

Large non-mass-dependent iron isotope fractionation in an oxic-anoxic transition zone of lake sediments

Liuting Song[1,2] ✉, Alfonso Mucci[3], Franck Poitrasson[4], Peter Dillon[5], Shuhai Xiao[6], Xiaodi Zheng[1,2], Yilong Song[7], Zhongliang Wang[8], Congqiang Liu[7] & Huiming Bao[9] ✉

Laboratory studies detected non-mass-dependent Fe-isotope fractionation during magnetotactic-bacteria-controlled iron (III) reduction, suggesting its potential as a biomineralization proxy. In nature, the preservation of the non-mass-dependent Fe-isotope signature may be difficult due to the abundance of other Fe-rich materials. Here we report a set of distinctly large non-mass-dependent Fe-isotope composition in the top 6.5 cm of the oxic-anoxic transition zone from a sediment core of Lake Aha, southwestern China. Negative $\Delta'^{57}Fe_d$-$\delta'^{56}Fe_d$ and positive $\Delta'^{57}Fe_d$-[Mn] correlations support that an abundance of manganese (IV) and ongoing sulfate reduction created a zone of Fe-limited porewaters in the top 6.5 cm of the sediment where magnetotactic bacteria thrived. Non-mass-dependent Fe-isotope signatures were not detected in a sediment core taken at a nearby site in the same lake where in the oxic-anoxic transition zone porewater Fe concentrations were orders-of-magnitude higher. The discovery of non-mass-dependent Fe-isotope signatures in natural sediment offers clues to detecting similar biosignatures.

Iron (Fe) is an essential element to nearly all living organisms. Whereas some bacteria may access Fe as a micronutrient, others derive energy from changes in its oxidation state[1,2]. The mineralization of Fe by magnetotactic bacteria (MTB) is one of the most intriguing biotic processes. A chain of magnetite (or greigite) crystals with a size range of 30–140 nm is generated inside the bacterial cell[3,4]. The crystals are often of stable single-magnetic domain with distinctive morphologies, indicating an intimate physiological control by MTB[4,5], and can be preserved in sediment as magnetofossils that can be interpreted as a signature of ancient[6,7] or possibly extraterrestrial life[8]. Recent culture experiments have highlighted that Fe isotopes undergo non-mass-dependent (NMD) fractionation during MTB-controlled magnetic Fe mineral formation[9,10], making NMD Fe-isotope anomalies a new and more specific biosignature of MTB activity than the morphology of the magnetite crystals or the δ'^{56}Fe signature alone (See Materials and methods for definitions). Nevertheless, despite numerous studies of Earth materials[11,12], distinct NMD Fe-isotope fractionation has not been reported in natural systems.

MTB are ubiquitous prokaryotes in aquatic systems and commonly concentrated at the upper oxic-anoxic transition zone (OATZ) of sediment[5,6]. Reasons why NMD Fe-isotope fractionation has not yet been detected in natural systems include the fact that Fe is a major constituent of sediment or rocks and, thus, the "anomalous" Fe if present would have been diluted by the large "normal" Fe pool. Furthermore, early diagenetic reactions may erase evidence of NMD Fe-isotope fractionation.

Whereas bulk sediments or pyrite minerals seem hopeless in recording MTB-controlled NMD Fe-isotope fractionation, porewater Fe may preserve evidence of MTB activity. Amor et al.[9,10,13] proposed that NMD Fe-isotope fractionation by MTB likely occurs when Fe redox reactions occur in the magnetosome membrane and the produced Fe(II) can then diffuse both into the magnetosome cytoplasm to produce magnetic Fe minerals and out of the cell to the growth medium. In nature, porewaters at the top OATZ could serve as a MTB "growth medium". When the MTB produced Fe(II) accounts for a considerable proportion of the porewater Fe, NMD Fe-isotope fractionation may be detectable.

[1]College of Water Sciences, Beijing Normal University, Beijing, China. [2]Engineering Research Center of Groundwater Pollution Control and Remediation Ministry of Education of China, Beijing Normal University, Beijing, China. [3]GEOTOP and Department of Earth and Planetary Sciences, McGill University, Montreal, QC, Canada. [4]Géosciences Environnement Toulouse, UMR 5563 CNRS/UPS/IRD, Toulouse, France. [5]Department of Chemistry, Trent University, Peterborough, ON, Canada. [6]Department of Geosciences, Virginia Tech, Blacksburg, VA, USA. [7]School of Earth System Science, Tianjin University, Tianjin, China. [8]Tianjin Key Laboratory of Water Resources and Environment, Tianjin Normal University, Tianjin, China. [9]International Center for Isotope Effects Research, School of Earth Sciences and Engineering, Nanjing University, Nanjing, China. ✉e-mail: ltsong@bnu.edu.cn; bao@nju.edu.cn

One potential target to detect NMD Fe fractionation is porewater in which MTB thrive and dissolved Fe is in limited supply. Lake Aha, in southwestern China, hosts an MTB-thriving zone at the top of the OATZ (Supplementary Fig. 1) found near the organic-rich sediment-water interface during the winter season when bottom waters are oxygenated[14–17]. The abundance and differential reactivity of electron acceptors such as Mn(IV), Fe(III), NO_3^-, and SO_4^{2-} in the lake sediments or water column generate diverse vertical redox zonation profiles within the sediment and, therefore, including porewater profiles that may provide an ideal setting to test our hypothesis. Indeed, we have discovered distinct NMD Fe-isotope fractionation in some of these porewater samples. We further examined the vertical distribution of electron acceptors in the porewaters at two sites in the same lake to investigate the preservation mechanism as well as origin of these large, NMD porewater Fe-isotope signatures.

Sampling site

Lake Aha have been shown to be a seasonally stratified lake by many recent studies[14–17] (Fig. 1). During summer stratification, dissolved O_2 is sufficiently removed from the bottom strata of Lake Aha and a pseudo redox boundary (DO, 2 mg.L^{-1}) is established over the hypolimnion (e.g., 10 m). The dissolved O_2 is as low as 0.1–0.2 mg L^{-1} near the sediment-water interface. In winter, after the fall overturning, the water column is well mixed with dissolved oxygen concentrations reaching as high as 4–9 mg L^{-1} near the sediment-water interface[17,18]. Meanwhile, bacterial sulfate reduction, Mn oxides reduction and dissimilatory iron reduction prevail in the sediments, a well-established OATZ is developed near the water/sediment interface with a ca. 0.5 cm reddish-brown surface layer in winter[15,16], where MTB thrived (Supplementary Fig. 1). Several mine dumps drain into the lake after the acidic effluents have been neutralized with lime[18], resulting in an abundance of reactive oxidants (electron acceptors, e.g., Fe oxides, Mn Oxides and SO_4^{2-}) in the water column and in the organic carbon-rich (2.5–4.5 OC%[19]) sediment of the lake. Youyu river is one of the tributaries drained with the mine dumps[18]. Fe and Mn were decoupled along the water flows from the shore (Youyu tributary) to downstream, near the lake center (Liangjiangkou) since the oxidation of Fe^{2+} by dissolved O_2 is nearly instantaneous, whereas the oxidation of Mn^{2+} by O_2 is relatively slow[20–23], resulting in a higher content of Mn_T and higher Mn_T/Fe_T at the Liangjiangkou station than that of Youyu station[15,24]. Short (<25 cm) sediment cores with an undisturbed sediment-water interface were recovered using a gravity corer, respectively, at Liangjiangkou station and Youyu station (Fig. 1).

Results

Porewater Fe, Mn, SO_4^{2-} concentrations in the OATZ

At Liangjiangkou, porewater Fe concentrations ([Fe_d]) are low, ranging from 1.2 to 2.9 μM over the top ~6.5 cm, below which they increase linearly until they reach a relatively constant value (100–120 μM) beneath 9.5 cm (Fig. 2A-a and Supplementary Table 1-A). Porewater NO_3^- concentrations were below the detection limit (3 μM) in the top 0–1.5 cm, although its concentration in the overlying water column was ~98 μM. Porewater Mn concentrations increase rapidly from below detection limit in the overlying waters to a peak value of 223 μM 1.5 cm below the sediment-water interface. They then decrease gradually with depth, reaching less than 5 μM below ~12.5 cm (Fig. 2A-a and Supplementary Table 1-A). Porewater SO_4^{2-} concentrations decrease steadily from 2.46 mM at the sediment-water interface to a minimum of 0.19 mM at 8.5 cm (Fig. 2A-c and Supplementary Table 1-A).

At Youyu, porewater Fe concentrations increase rapidly below the sediment-water interface, peak at ~100 μM by 1.5 cm and decrease to less than 20 μM below 3.5 cm (Fig. 2B-a and Supplementary Table 1-B). They are much higher than in the Liangjiangkou sediment (Supplementary Fig. 2A). In contrast with the porewater profiles at Liangjiangkou, the porewater Mn concentration at Youyu peaks at 2.5 cm, close to but slightly deeper than the porewater Fe peak. According to measurements carried out using the Diffusive Gradients in Thin Films Technique (DGT), porewater sulfide concentrations peak below 8 cm[25].

Triple Fe isotope compositions ($\delta'^{56}Fe_d$ and $\Delta'^{57}Fe_d$) of porewater Fe in the OATZ

At Liangjiangkou, porewater $\delta'^{56}Fe_d$ values in the top 6.5 cm range from −4.57‰ to −2.59‰, with the most negative value located in the topmost layer (0–0.5 cm) (Fig. 2A-d and Supplementary Table 2-A). Porewaters extracted beneath 6.5 cm have $\delta'^{56}Fe_d$ values ranging from −2.53 to −0.35‰, all less negative than those at shallower depths. In the top 6.5 cm, porewater $\Delta'^{57}Fe_d$ (See Materials and methods for definitions) ranges from +0.44‰ to +1.60‰, displaying large NMD Fe-isotope anomalies. Beneath 6.5 cm, the $\Delta'^{57}Fe_d$ remains between −0.06 and +0.04‰ (Fig. 2A-e and Supplementary Table 2-A), displaying mass-dependent triple Fe-isotope fractionation within the uncertainty of the measurements (<±0.14‰, 2 SD) (Supplementary Methodology and Supplementary Fig. 3). There is a good negative correlation ($r^2 = 0.64$) among the porewater data in the top 6.5 cm of the core in $\Delta'^{57}Fe_d$-$\delta'^{56}Fe_d$ space (Fig. 3B). Data of top layer porewaters (≤6.5 cm) fall into one cluster with lower $\delta'^{56}Fe_d$ and positive $\Delta'^{57}Fe_d$ under Fe-limited conditions, while data of deeper layer porewaters (>6.5 cm) fall into another cluster with higher $\delta'^{56}Fe_d$ and no distinct NMD ^{57}Fe signature was observed under Fe-rich conditions (Fig. 3C, D). At Youyu, porewater $\delta'^{56}Fe_d$ ranges from −2.0‰ to −0.74‰ between 0.5 and 13.5 cm, with no distinct NMD ^{57}Fe anomaly (Fig. 2B-c and Supplementary Table 2-B).

Other concentrations and Fe isotope data in the OATZ

Fe_T/Al can be used to determine their authigenic enrichment since Al is conservative detrital element while Fe is redox sensitive element and reactive Fe could be reduced and precipitated as authigenic Fe minerals, e.g., FeS, under suboxic and anoxic conditions[26–28]. Similarly, Mn could undergo diagenetic remobilization and reprecipitate as Mn oxides under suboxic and oxic conditions near the sediment surface[29]. At Liangjiangkou, bulk sediment Fe (Fe_T), Mn (Mn_T), S (S_T), Mn_T/Al, Fe_T/Al, Mn_T/Fe_T, and $\delta'^{56}Fe_T$ as well as $\delta'^{56}Fe_{HCl}$ (i.e., 1M-HCl extractable) profiles provide additional constraints on the redox zonation in the upper OATZ. Some of the outstanding features are highlighted here. (1) Fe_T is nearly constant (from 1.05 to 1.45 mmol/g) within the top 6.5 cm of the core, peaks (3.14 mmol/g) at 8.5–10.5 cm, and averages twice that content in the deeper section than in the top 6.5 cm (Supplementary Table 1-A). The vertical profiles of Fe_T/Al, Mn_T/Al, and Mn_T display similar patterns, with constant and low values in the top 6.5 cm of the sediment, peaking at 8.5–10.5 cm, and decreasing to low or even lower values than in the top 6.5 cm below (Fig. 2A-b, f and Supplementary Fig. 2). (2) Mn_T/Fe_T peaks in the topmost 0.5 cm, decreases progressively downcore and becomes very small (average at 0.02) below 10.5 cm (Fig. 2A-f). This vertical pattern broadly mimics the $\Delta'^{57}Fe_d$ profile and mirrors that of $\delta'^{56}Fe_d$ over the entire ~25 cm long core (Fig. 2A-d, e). (3) S_T is higher than 0.5% in the top 10.5 cm of the core, but lower beneath 10.5 cm (Fig. 2A-c). 4) Both $\delta'^{56}Fe_T$ and $\delta'^{56}Fe_{HCl}$ display a narrow range of values, from −0.46‰ to −0.60‰ and from −1.17‰ to −1.39‰, respectively, in the top 6.5 cm, and show a notable negative excursion (to −1.72‰ and −2.02‰ and to −2.42‰ and −2.70‰, respectively) at 8.5 and 10.5 cm before they return to nearly identical and constant values at depth (Fig. 2A-d and Supplementary Table 2-A) with no discernable NMD ^{57}Fe anomaly throughout the Liangjiangkou core (Fig. 2A-e). At Youyu, Mn_T is much lower (up to one order of magnitude at some depths) than at Liangjiangkou, with an average Mn_T/Fe_T of 0.07 and 0.29, respectively, in the top 3.5 cm (Fig. 2B-b, Supplementary Table 1-B and Supplementary Fig. 2A).

Discussion

An unusual redox zonation resulting in low porewater Fe concentrations at the top OATZ

MTB require both iron and lower level of oxygen to produce their intracellular nano-sized magnetic crystals, limiting the optimum MTB growth zone to the upper part of the OATZ in a water column[30,31], soil[32], or sediment[33,34]. In many organic-rich sediments, Fe(III) reduction inevitably leads to the accumulation of porewater Fe(II) in the upper OATZ but, at the Liangjiangkou station in Lake Aha, a set of environmental factors have

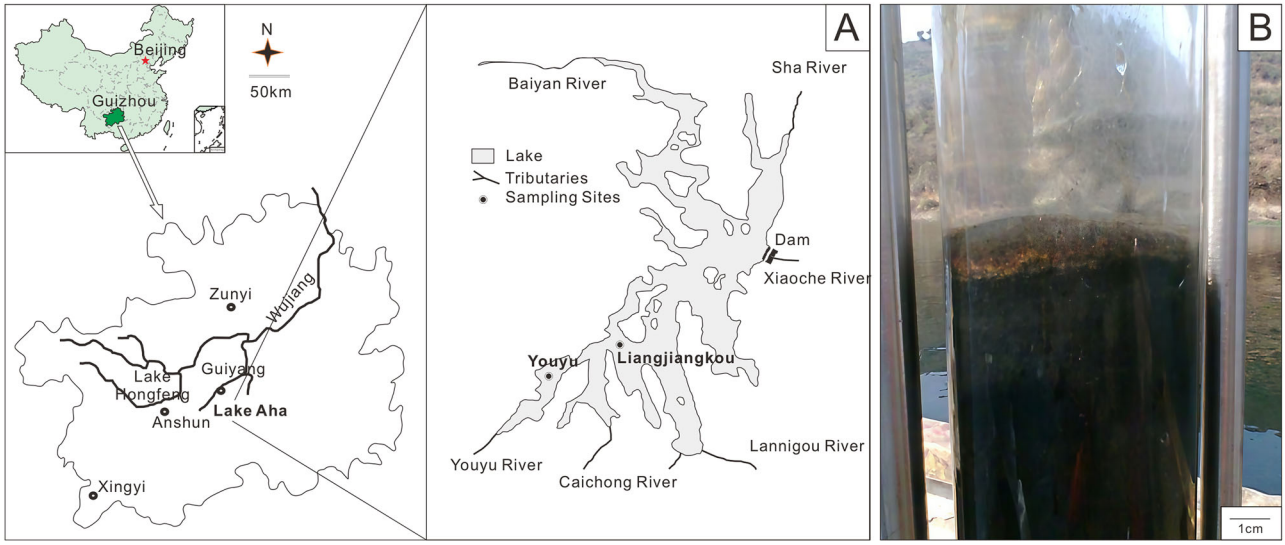

Fig. 1 | Map of Sampling locations in Lake Aha, Guizhou, southwestern China. A Sampling sites of the two sediment cores, Liangjiangkou and Youyu stations in Lake Aha. **B** Photo of the sediment core sampled in this study, with an undisturbed sediment-water interface and an oxic surface layer, where a well-established OATZ was developed.

combined to generate Fe-limited porewaters in the top 6.5 cm of the lake sediments.

In a classical, thermodynamically-controlled redox sequence, organic matter is first oxidized by dissolved O_2, followed by nitrate, Mn (IV), Fe(III), and then sulfate[22,35–37] (Fig. 4). At Liangjiangkou, a distinct redox zonation developed within the sediment, as indicated by the vertical solid and solute profiles (Fig. 2 and Supplementary Table 1-A). At this site, the redox zonation started with O_2 and nitrate being used as the electron acceptors in the top 0–1.5 cm of the sediment, followed by Mn-oxide reduction and sulfate reduction at 0.5–8.5 cm, whereas Fe-oxide reduction was only apparent below 7.5 cm (Fig. 4). This redox zonation differs from the classical thermodynamic sequence in that Fe(III) reduction does not occur immediately beneath the Mn(IV) reduction zone but after sulfate reduction has been initiated. The apparent "violation" of the thermodynamic sequence must be driven by kinetic factors, e.g., availability of degradable organic carbon, reactivity of Fe(III) minerals as well as energetic factors pertinent to the microbial ecology and physiology[38,39]. It is noteworthy that the low and nearly constant porewater Fe concentrations (1.2–2.9 μM) average only ~3 times of the detection limit (0.5 μM) in the top 6.5 cm, much lower than those observed at greater depth (average 110 μM) (Fig. 2A-a, Supplementary Fig. 2 and Supplementary Table 1-A). Note, however, that the measured porewater Fe could include soluble organic-Fe(III) species and even some colloidal magnetite grains in addition to soluble Fe(II)[40,41].

We believe that the dearth of porewater Fe in the top 6.5 cm of the Liangjiangkou core reflects the combination of three factors that contrast with profiles in the Youyu core: (1) Delayed reductive dissolution of Fe(III) minerals because of their limited abundance and reactivity ($Fe(III)_{HCl}$, $Fe(III)_{HCl}/Fe_{HCl}$, Supplementary Fig. 4 and Supplementary Table 1-A) within this depth interval; (2) Accumulation of porewater Fe(II) in the top OATZ inhibited by the abundance of solid Mn(IV) phases (Mn_T, see Fig. 2A-b, B-b and Supplementary Tables 1-A, B). In winter, after the fall overturning, Mn(IV, III) oxides precipitated at the sediment-water interface forming a Mn-rich layer in the top OATZ[15,17,42] (Mn_T and Mn/Al, Fig. 2A-b, f and Supplementary Table 1-A). Mn oxides can readily oxidize Fe(II) to an amorphous Fe(III) oxide[22,43], as indicated by the elevated [Mn_d] (see Fig. 2A-a, B-a); (3) The very early onset of sulfate reduction (Fig. 2A-c) and sequestration of Fe(II) as insoluble and bio-inaccessible sulfides ($Fe(II)_{HCl}$, Supplementary Fig. 4; S_T, Fig. 2A-c), which is consistent with the results in previous studies[19,44] since sulfate reduction prevails in the top sediment layers[15,16,45]. In addition, the early onset of sulfate reduction in the OATZ would prevent the accumulation of porewater Fe(II) and its upward diffusion to the top of the OATZ where it could be oxidized and Fe(III) phases could be diagenetically recycled. This interpretation is supported by the high porewater Fe concentrations observed below 11 cm, i.e., beneath the sulfate reduction zone and by the nearly constant Fe_T/Al that is similar to that of the settling particulates[18] throughout the core, except within the 8–11 cm sediment interval where diagenetically remobilized Fe is accumulating (Fig. 2A-a, f and Supplementary Table 1-A). It appears that porewater Fe and Mn are precipitated out at 8–11 cm, likely in the form of FeS_x with Mn (II) strongly adsorbed to FeS[46–48].

Interpretation of the Liangjiangkou redox zonation is only possible by considering both thermodynamic and kinetic constraints among the competing microbial consortiums[49] but impractical at this time as many kinetic (e.g., Michaelis-Menten) parameters are either uncalibrated in controlled experiments or untested in natural environments. Qualitatively, the solid and solute distributions in the Liangjiangkou sediment point to a consistent scenario, i.e., porewater Fe concentrations are limited in the top 6.5 cm of the sediment due to the limited abundance and reactivity of Fe(III) minerals (low $Fe(III)_{HCl}$ and $Fe(III)_{HCl}/Fe_{HCl}$), the abundance of Mn(IV) as well as the early onset of sulfate reduction and precipitation of iron sulfides (elevated $Fe(II)_{HCl}$ and S_T).

Anomalous isotopic composition of porewater Fe in the top OATZ: an Fe-limited model

The negative correlation between $\Delta^{57}Fe_d$ and $\delta^{56}Fe_d$ (Fig. 3B) in the top 6.5 cm of the Liangjiangkou sediment can be explained by a two-endmember mixing model. In the mixing model, endmember 1 would be Fe_{HCl} with a $\delta^{56}Fe$ of −1.3‰ and a $\Delta^{57}Fe$ of 0.0‰, as given by the intercept of the linear least-squares regression line in Fig. 3B, and endmember 2 would be the product of MTB-controlled Fe(III) reduction with a $\delta^{56}Fe < -4.57$‰ and a $\Delta^{57}Fe > +1.60$‰, as indicated by the Group 2 data array in Fig. 3B. This pattern fits well with the proposed model[9,10] in which Fe in the growth media, likely released from MTB cells, has a more negative $\delta^{56}Fe$ value than the source Fe or Fe_{HCl}. It also implies, as observed, that the growth media should yield a positive $\Delta^{57}Fe$ rather than a zero $\Delta^{57}Fe$ value for the source Fe or Fe_{HCl}. Our observed trends in $\Delta^{57}Fe_d$-$\delta^{56}Fe_d$ space suggest that NMD Fe-isotope fractionation during the MTB-controlled Fe(III) reduction to Fe(II) in the cell's lysate favors the production of lighter Fe isotopes, but the $\delta^{57}Fe$ signature is higher than the mass-dependent rule would dictate. In addition, the magnetosome crystals, bearing lower $\delta^{56}Fe$ but positive $\Delta^{57}Fe$ values, could release into the porewater upon cell lysis because of the small sizes of these crystals (usually, 30–140 nm in size[4,50]), lower than the 0.45 μm pores. These colloidal magnetite grains are soluble in acidic conditions, could also "contaminate" the porewater samples.

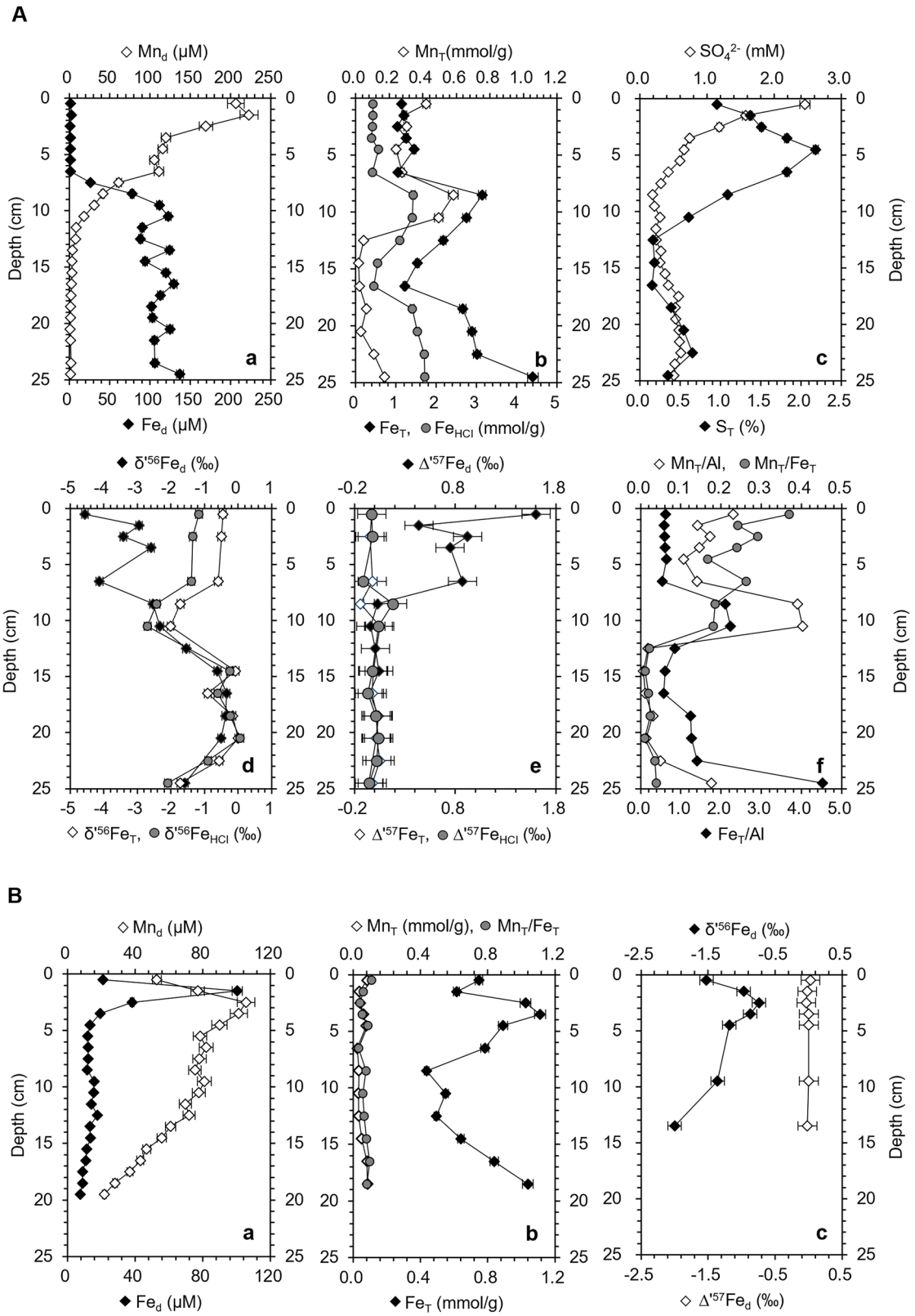

Fig. 2 | Vertical chemical and Fe-isotope profiles of porewaters or sediments of Lake Aha. A Liangjiangkou station. **B** Youyu station. Subscript "d" stands for dissolved (porewater) species, subscript "HCl" for Fe extracted by the 1 M HCl method, and subscript "T" for elements in the bulk sediments. Data labels are identified by a symbol to their left and adjacent to their corresponding horizontal axis. Errors bars for Fe, Mn, SO_4^{2-} and S_T are ±3%, ±5%, ±3% and ±1.5%, respectively, while error bars for δ^{56}Fe, δ^{57}Fe, and Δ^{57}Fe are ±0.10‰, ±0.16‰ and ±0.14‰ (2 SD), respectively.

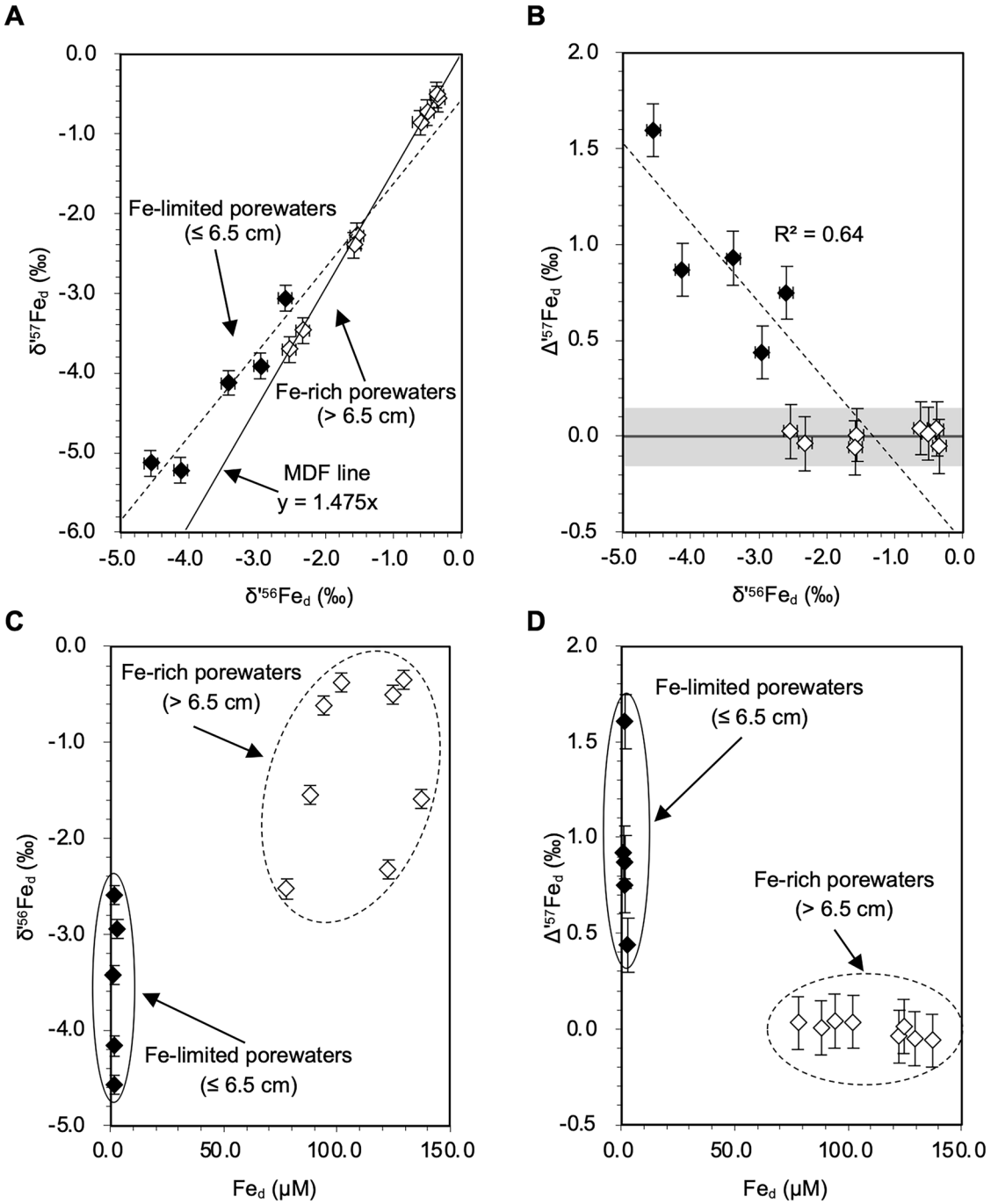

Fig. 3 | Isotopic compositions of porewater Fe and their relationships with each other and with the dissolved Fe concentrations of the Liangjiangkou core. **A** $\delta^{'57}Fe_d$ versus $\delta^{'56}Fe_d$ for all data from the top ~25 cm of the core. Group 1 data (hollow) were from depths below the Mn reduction zone (>6.5 cm) and they fall closely along a high-temperature-limit mass-dependent fractionation (MDF) line defined by a slope of 1.475 (solid line). Group 2 data (filled) were from the top 6.5 cm (≤6.5 cm) of the core and display significant deviations from the MDF line. **B** $\Delta^{'57}Fe_d$ versus $\delta^{'56}Fe_d$ for all data from the top ~25 cm of the core with the $\Delta^{'57}Fe$ being more positive with decreasing $\delta^{'56}Fe$ porewater values in the top 6.5 cm ($R^2 = 0.64$). The gray horizontal band (±0.14‰, 2 SD) covers samples with no distinct NMD Fe isotope signature. A linear least-squares regression line through samples of Group 2 intersects with samples of Group 1 at a $\delta^{'56}Fe$ of −1.3‰. **C** $\delta^{'56}Fe_d$ versus Fe_d diagram. Data of Fe-limited porewaters (≤6.5 cm) fall into one cluster with $\delta^{'56}Fe_d$ lower than those of Fe-rich porewaters (>6.5 cm) in another cluster. **D** $\Delta^{'57}Fe_d$ versus Fe_d diagram. Data of Fe-limited porewaters (≤6.5 cm) fall into one cluster with positive $\Delta^{'57}Fe_d$ while those of Fe-rich porewaters (>6.5 cm) with no distinct NMD Fe isotope signatures fall into another cluster. Error bars for $\delta^{'56}Fe$, $\delta^{'57}Fe$, and $\Delta^{'57}Fe$ are ±0.10‰, ±0.16‰ and ±0.14‰ (2 SD), respectively.

This NMD fractionation mechanism requires Fe-limited porewaters in order to preserve the NMD signatures, i.e., to avoid dilution of the NMD signature by Fe(II) resulting from dissimilatory Fe(III) reduction. This mechanism could be tested by measuring the triple Fe isotope composition of the MTB-generated magnetite. In this mixing model, the Fe(III) to Fe(II) reduction mechanism proposed by Amor and colleagues[9,10] would yield a positive $\Delta^{'57}Fe$ for the magnetite. The nucleus-electron spin-pairing in ^{57}Fe is likely responsible for the observed NMD Fe- isotope fractionation[9,51], a hypothesis that would generate no NMD anomaly in the corresponding $\delta^{58}Fe$ values due to the lack of nuclear spin in ^{58}Fe, ^{56}Fe, or ^{54}Fe. Such a test would require a scaled-up sampling protocol due to the unusually low porewater Fe concentrations in the top 6.5 cm of the Liangjiangkou core.

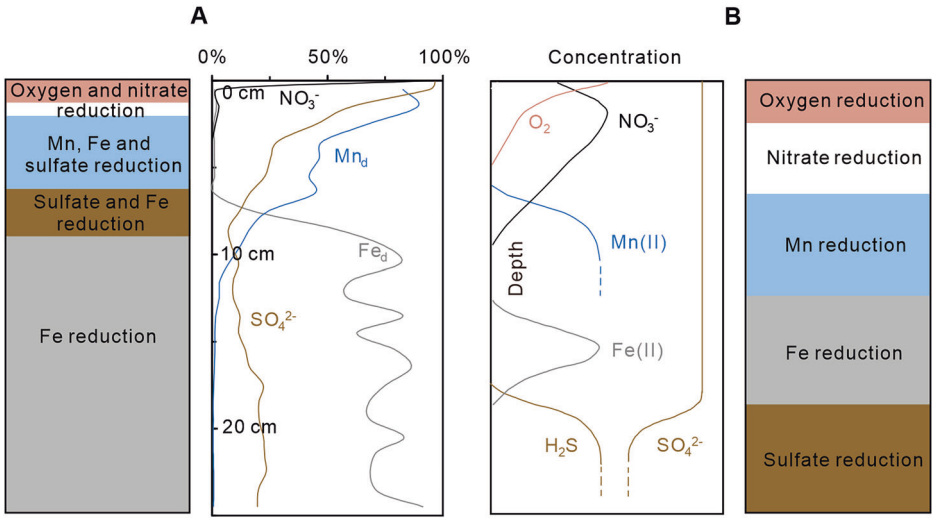

Fig. 4 | Redox zonation models. A A model of the redox zonation and the consequent Fe-limited porewaters in the top 6.5 cm at the Liangjiangkou station core, Lake Aha. Individual ion concentrations are normalized to their respective, highest concentrations (NO_3^- = 100 μM; Mn_d = 250 μM; Fe_d = 150 μM; and SO_4^{2-} = 2.6 mM) on the horizontal axis. Note the overlap of the sulfate reduction zone with the Mn and Fe reduction zones. **B** A classic thermodynamics-based redox zonation, taken from Froelich et al.[35] and Madison et al.[37] for coastal marine sediment. Scales of the x and y axes in B are arbitrary.

An array of element/ion concentrations and triple Fe isotope data provide strong and consistent support for this Fe-limited model. (1) The three solid samples in the top 6.5 cm of the Liangjiangkou sediment core have an average $\delta^{56}Fe_{HCl}$ of −1.3‰ and $\delta^{56}Fe_T$ of −0.5‰ (Supplementary Table 2-A), in agreement with the expected Fe_{HCl} isotopic fractionation relative to the parent Fe(III) oxides[52]. (2) The Fe_T/Al peaked at 8–11 cm below the sediment-water interface, where the mobile Fe was sequestered as sulfides upon diffusion from the underlying reducing sediments and where the most negative $\delta^{56}Fe$ values for bulk sediment (−1.72‰ to −2.02‰) and for Fe_{HCl} (−2.42‰ to −2.70‰) were observed (Figs. 2A-d, f and Supplementary Table 2-A). (3) The $\delta^{56}Fe$ in the top 6.5 cm of the bulk sediment (−0.60‰ to −0.46‰) and HCl-extract (Fe_{HCl} = −1.39‰ to −1.17‰) vary over narrow ranges (Fig. 2A-d and Supplementary Table 2-A), suggesting that the top 6.5 cm of the sediment behaves as a nearly closed system with respect to Fe remobilization, without substantial Fe being shuttled to or from deeper sediments.

The proposed Fe-limited model predicts that porewater triple Fe-isotope compositions will display mass-dependent fractionation if the porewater Fe content is high in the OATZ. The Youyu station data provide a test of this prediction. Porewater Fe concentrations at Youyu were 1–2 orders of magnitude higher than at Liangjiangkou in the top OATZ (Supplementary Fig. 2A). Both porewater Fe and Mn reached peak concentrations close to the surface (Fig. 2B-a and Supplementary Table 1-B) and displayed a peak porewater sulfide content below 8 cm[25], a redox zonation that closely mimics the classical thermodynamic sequence. All 7 porewater Fe samples measured in the top 13 cm of this core exhibit mass-dependent Fe-isotope signatures (Fig. 2B-c and Supplementary Table 2-B). The Mn_T content in the Youyu sediment is, on average, 5 times lower than in the top 6.5 cm of the Liangjiangkou sediment core (Supplementary Fig. 2A) where NMD Fe-isotope signatures are detected in porewater Fe.

Only a few triple Fe-isotope measurements of porewater Fe can be found in the literature[53–57]. None of these studies have reported NMD Fe- isotope anomalies. A common feature is that the porewater Fe concentrations in the top of the OATZ of all the studied sites were ~30 to 1000 times higher than at the Liangjiangkou station in Lake Aha. For example, the two marine sediments off the coast of California display a nearly classical redox zonation, show similarly negative $\delta^{56}Fe$ values of porewater Fe as those in Liangjiangkou but no porewater Fe NMD anomaly[56]. Hence, we believe that the low porewater Fe concentrations in the first 6.5 cm of the sediment in the Liangjiangkou core and, therefore, the large fraction of the porewater Fe pool involved in the MTB-controlled Fe redox cycling within this interval allows for the preservation of the NMD Fe-isotope fractionation signature.

Implications for geological records

If the origin of the NMD Fe-isotope signatures is the MTB-controlled Fe redox cycling and transport, we must first look for environments where MTB thrive and where the accumulation of porewater Fe is minimal. The presence of bioavailable organic matter would be required to sustain these communities. If the joint effect of abundant Mn (IV), early onset of sulfate reduction and consequent sequestration of Fe(II) as solid sulfides is the key to maintain porewater Fe concentrations below 3 μM at the top of the OATZ, both Mn(IV) and SO_4^{2-} must be available in the organic-rich sediment. These two prerequisite conditions may not be hard to meet in modern sedimentary environments. Future efforts can be directed at finding other natural environments where NMD Fe-isotope fractionation can be documented and conditions conducive to the process as well as preservation of the signal can be identified. Porewaters are not preserved in the rock record but the isotopic composition of porewater-Fe may be recorded in some authigenic minerals (e.g., carbonate, chert, and barite) precipitated from Fe-limited porewaters where MTB thrived.

Despite some uncertainties on Fe-isotope fractionation and reservoir-transport effects within and among porewater systems, the vertical distribution of electron acceptors, their reaction products, and Fe-isotope data in Lake Aha sediment profiles paint a consistent scenario: (1) Large NMD Fe-isotope fractionation resulting from the activity of MTB can be preserved in the porewater Fe at the top of the OATZ; (2) A prerequisite for the preservation of the NMD Fe-isotope signature in porewater is its low Fe concentration in MTB-thriving sediments, a condition that can be facilitated by the presence of a high Mn content and an early onset of microbial sulfate reduction in the top OATZ of the sediment.

Materials and methods

All samples were handled and treated following standard protocols established in the community (see references below and further details in Supplementary Methodology).

Sample handling

All polypropylene (PP) tubes and bottles used in the field and in the laboratory were soaked for 48 h in a 6 M HCl bath and subsequently rinsed repeatedly with 18.2 MΩ Milli-Q water (no HCl rinsing for sulfate measurement). Sediment cores were taken from a boat using a polymethylmethacrylate tube with a 5.9 cm internal diameter. Within 3 h of recovery, the lake sediment cores were sectioned at 1-cm intervals on shore in N_2-filled glove bags and kept in 50 mL screw-cap PP centrifuge tubes. The porewater was then extracted by centrifugation at about 2000 × *g* for 20 min. The centrifuge tubes were returned to a N_2-filled glove bag where the supernatant was filtered through a 0.45 μm Millipore HA membrane with a 50-mL plastic syringe. Filtered porewaters for metal ion concentrations and

Fe isotope analyses were acidified using ultrapure HNO_3 to pH < 2 whereas those for sulfate concentration measurements were diluted with Milli-Q water. The solid sediments in the 50-mL centrifuge tubes were freeze-dried and ground into powder (<200 mesh) with an acid-cleaned agate mortar and pestle.

Analysis of sediment and porewaters

The freeze-dried sediments were reacted with a 1 M HCl solution at room temperature for 16 h to determine the amount of reactive Fe, following the method described by Huerta-Diaz and Morse[58]. Aliquots of porewaters, HCl extracts and bulk sediments were digested with aqua regia and concentrated HF and then purified twice using an AGMP-1 anionic resin (Bio-Rad, 100-200 mesh, chloride form), according to an established protocol (See Supplementary Methodology). Porewaters as well as the HCl-extracts and digested-sediment solution Fe, Mn, and Al concentrations were determined at the Chinese Academy of Geological Sciences by ICP-AES (Thermo Fisher, TJA-IRIS-Advantage) with a detection limit of 0.5 μM, 0.2 μM, and 3 μM, or uncertainty of ±3%, ±5%, and ±7%, respectively. Porewater NO_3^- and SO_4^{2-} concentrations were determined by ion chromatography (Dionex, ICS-90) at the Chinese Academy of Sciences laboratory with an uncertainty of 3% and respective detection limits of 2 μM and 3 μM. Total S was determined using an elemental analyzer (Wanlianda, CS902) with a precision better than 0.1% and an uncertainty of 1.5%.

Triple Fe-isotope compositions

Fe isotope measurements were conducted on a Neptune MC-ICP-MS (Thermo-Fisher, Germany) at the Water Quality Centre, Trent University (Canada) and on a Neptune Plus MC-ICP-MS (Thermo Fisher, Germany) at the Beijing Createch Testing Technology Co., Ltd. (China). The purified sample solutions were introduced into an argon plasma by a peristaltic pump with an ion beam of 9 V on ^{56}Fe for a 3.0 mg/L Fe solution on the Neptune Plus MC-ICP-MS or by a Cetac Aridus Desolvating nebulizer with an ion beam of 12 V on ^{56}Fe for a 0.2 mg/L Fe solution on the Neptune MC-ICP-MS. All measurements were carried out in high-resolution mode, a mass resolving power (m/Δm) of ~9000 for the Neptune MC-ICP-MS and ~7000 for the Neptune Plus MC-ICP-MS, so that the isobaric interferences (e.g., $^{40}Ar^{14}N^+$ on $^{54}Fe^+$, $^{40}Ar^{16}O^+$ on $^{56}Fe^+$ and $^{40}Ar^{16}OH^+$ on $^{57}Fe^+$) were resolvable (Supplementary Fig. 5). The standard-sample bracketing (SSB) method was applied with the reference Fe standard IRMM-014 throughout the study to minimize instrumental mass bias. Given the low porewater Fe concentrations and, thus, the low ^{58}Fe signal on the mass spectrometer, we did not attempt to measure the $\delta'^{58}Fe$ for the entire set of samples. The performance of the Neptune instrument was assessed by repeated measurements of an internal laboratory reference (ICP Fe, $n = 12$) and a purified sample solution (porewater extracted from 8.5 cm in the Liangjiangkou core, $n = 27$). The average isotopic compositions, obtained in high-resolution mode under optimized conditions, are $\delta'^{57}Fe = -0.15 \pm 0.12‰$ (2 SD) and $\delta'^{56}Fe = -0.12 \pm 0.09‰$ (2 SD) for the ICP-Fe solution; and $\delta'^{57}Fe = -3.70 \pm 0.16‰$ (2 SD), $\delta'^{56}Fe = -2.53 \pm 0.10‰$ (2 SD) and $\Delta'^{57}Fe = 0.03 \pm 0.14‰$ (2 SD) for the porewater (Supplementary Fig. 3). The precision of measurements on the Neptune Plus, operated in high-resolution mode under optimized conditions, was derived from repeated measurements of an internal laboratory reference (CAGS-Fe, $n = 71$) for which the average $\delta'^{57}Fe = 1.17 \pm 0.14‰$ (2 SD) and $\delta'^{56}Fe = 0.80 \pm 0.08‰$ (2 SD) (Supplementary Fig. 3), values that are statistically identical to its reported isotopic compositions, $\delta'^{57}Fe = 1.20 \pm 0.13‰$ (2 SD) and $\delta'^{56}Fe = 0.83 \pm 0.07‰$ (2 SD)[59]. Further testing revealed that the NMD Fe-isotope signatures are analytically robust (see Supplementary Methodology and Supplementary Table 3 for detail). The robustness of the triple Fe-isotope compositions is also supported by the smooth distribution pattern of the data (Supplementary Fig. 3) obtained by two different spectrometers in two different laboratories.

Fe isotope notations

Fe isotope data are reported as $\delta'^{x}Fe$ ($\delta'^{56}Fe$, $\delta'^{57}Fe$) in parts per thousand (per mil, ‰) deviations relative to IRMM-014.

$$\delta'^{56}Fe = \ln[(^{56}Fe/^{54}Fe)_{sample}/(^{56}Fe/^{54}Fe)_{IRMM-014}]$$

$$\delta'^{57}Fe = \ln[(^{57}Fe/^{54}Fe)_{sample}/(^{57}Fe/^{54}Fe)_{IRMM-014}]$$

$$\Delta'^{57}Fe = \delta'^{57}Fe - 1.475 \times \delta'^{56}Fe$$

$$\delta' = \ln(1 + \delta)$$

Reporting summary

Further information on research design is available in the Nature Portfolio Reporting Summary linked to this article.

Data availability

All data are available in the main text and the Supplementary Information or available via Figshare at https://doi.org/10.6084/m9.figshare.30375154.v3.

Received: 16 May 2025; Accepted: 20 October 2025;
Published online: 26 November 2025

References

1. Kendall, B., Anbar, A. D., Kappler, A. & Konhauser, K. O. The Global Iron Cycle. in *Fundamentals of Geobiology* 65–92 (John Wiley & Sons, Ltd, 2012).
2. Melton, E. D., Swanner, E. D., Behrens, S., Schmidt, C. & Kappler, A. The interplay of microbially mediated and abiotic reactions in the biogeochemical Fe cycle. *Nat. Rev. Microbiol.* **12**, 797–808 (2014).
3. Bazylinski, D. A. & Frankel, R. B. Magnetosome formation in prokaryotes. *Nat. Rev. Microbiol.* **2**, 217–230 (2004).
4. Faivre, D. & Schüler, D. Magnetotactic bacteria and magnetosomes. *Chem. Rev.* **108**, 4875–4898 (2008).
5. Komeili, A. Molecular mechanisms of compartmentalization and biomineralization in magnetotactic bacteria. *FEMS Microbiol. Rev.* **36**, 232–255 (2012).
6. Kopp, R. E. & Kirschvink, J. L. The identification and biogeochemical interpretation of fossil magnetotactic bacteria. *Earth Sci. Rev.* **86**, 42–61 (2008).
7. Jimenez-Lopez, C., Romanek, C. S. & Bazylinski, D. A. Magnetite as a prokaryotic biomarker: a review. *J. Geophys. Res. Biogeosci*. **115**, 1–19 (2010).
8. McKay, C. P., Friedmann, E. I., Frankel, R. B. & Bazylinski, D. A. Magnetotactic bacteria on Earth and on Mars. *Astrobiology* **3**, 263–270 (2003).
9. Amor, M. et al. Mass-dependent and -independent signature of Fe isotopes in magnetotactic bacteria. *Science* **352**, 705–708 (2016).
10. Amor, M. et al. Iron uptake and magnetite biomineralization in the magnetotactic bacterium Magnetospirillum magneticum strain AMB-1: an iron isotope study. *Geochim. Cosmochim. Acta* **232**, 225–243 (2018).
11. Dauphas, N., John, S. G. & Rouxel, O. Iron isotope systematics. *Rev. Mineral. Geochem.* **82**, 415–510 (2017).
12. Beard, B. L. & Johnson, C. M. Fe isotope variations in the modern and ancient earth and other planetary bodies. *Rev. Mineral. Geochem.* **55**, 319–357 (2004).
13. Amor, M. et al. Magnetochrome-catalyzed oxidation of ferrous iron by MamP enables magnetite crystal growth in the magnetotactic bacterium AMB-1. *Proc. Natl. Acad. Sci. USA* **121**, e2410245121 (2024).

14. He, T. et al. The impact of acid mine drainage on the methylmercury cycling at the sediment–water interface in Aha Reservoir, Guizhou, China. *Environ Sci Pollut Res.* **22**, 5124–5138 (2015).
15. Wang, F. *The geochemical behavior of trace metals near the water–sediment interface in seasonally anoxic lakes*. Ph.D. thesis, University of Chinese Academy of Sciences, China. (2003).
16. Wang, F., Liu, C., Liang, X. & Wei, Z. Microbial activities at the sediment–water interface and their impact on remobilization and enrichment of trace elements in Aha Lake, Guizhou, China. *Chin. Sci. Bull.* **48**, 2073–2078 (2003).
17. Chen, Q. et al. Manganese(III) dominants the mobilization of phosphorus in reducing sediments: evidence from Aha reservoir, Southwest China. *Sci. Total Environ.* **954**, 176564 (2024).
18. Song, L. et al. Iron isotope fractionation during biogeochemical cycle: Information from suspended particulate matter (SPM) in Aha Lake and its tributaries, Guizhou, China. *Chem. Geol.* **280**, 170–179 (2011).
19. Findlay, A. J. et al. Sulfide oxidation affects the preservation of sulfur isotope signals. *Geology* **47**, 739–743 (2019).
20. Balistrieri, L. S., Murray, J. W. & Paul, B. The biogeochemical cycling of trace metals in the water column of Lake Sammamish, Washington: Response to seasonally anoxic conditions. *Limnol. Oceanogr.* **37**, 529–548 (1992).
21. Davison, W. Iron and manganese in lakes. *Earth Sci. Rev.* **34**, 119–163 (1993).
22. Nealson, K. H. & Saffarini, D. Iron and manganese in anaerobic respiration: environmental significance, physiology, and regulation. *Annu. Rev. Microbiol.* **48**, 311–343 (1994).
23. Morgan, J. J. Kinetics of reaction between O2 and Mn(II) species in aqueous solutions. *Geochim. Cosmochim. Acta* **69**, 35–48 (2005).
24. Wang, F., Liu, C., Liang, X., Wei, Z. & Li, J. Acid mining drainage impacts on the separation between iron and manganese in sediments of the Aha Lake, Guizhou Province. *Environ. Sci.* **26**, 135–140 (2005).
25. Chen, Q. *In-situ, high resolution study on the mechanism of internal phosphorus release at the sediment-water interface in deep-water reservoirs, Yunnan-Guizhou Plateau, China.* M.S. thesis, University of Chinese Academy of Sciences, China (2019).
26. Lyons, T. W., Werne, J. P., Hollander, D. J. & Murray, R. W. Contrasting sulfur geochemistry and Fe/Al and Mo/Al ratios across the last oxic-to-anoxic transition in the Cariaco Basin, Venezuela. *Chem. Geol.* **195**, 131–157 (2003).
27. Lyons, T. W. & Severmann, S. A critical look at iron paleoredox proxies: new insights from modern euxinic marine basins. *Geochim. Cosmochim. Acta* **70**, 5698–5722 (2006).
28. Fehr, M. A., Andersson, P. S., Hålenius, U. & Mörth, C.-M. Iron isotope variations in Holocene sediments of the Gotland Deep, Baltic Sea. *Geochim. Cosmochim. Acta* **72**, 807–826 (2008).
29. Paul, K. M. et al. Revisiting the applicability and constraints of molybdenum- and uranium-based paleo redox proxies: comparing two contrasting sill fjords. *Biogeosciences* **20**, 5003–5028 (2023).
30. Bazylinski, D. A. et al. Controlled biomineralization of magnetite (Fe(inf3)O(inf4)) and Greigite (Fe(inf3)S(inf4)) in a magnetotactic bacterium. *Appl. Environ. Microbiol.* **61**, 3232–3239 (1995).
31. Simmons, S. L., Sievert, S. M., Frankel, R. B., Bazylinski, D. A. & Edwards, K. J. Spatiotemporal distribution of marine magnetotactic bacteria in a seasonally stratified coastal salt pond. *Appl. Environ. Microbiol.* **70**, 6230–6239 (2004).
32. Fassbinder, J. W. E., Stanjekt, H. & Vali, H. Occurrence of magnetic bacteria in soil. *Nature* **343**, 161–163 (1990).
33. Blakemore, R. Magnetotactic bacteria. *Science* **190**, 377–379 (1975).
34. Flies, C. B. et al. Diversity and vertical distribution of magnetotactic bacteria along chemical gradients in freshwater microcosms. *FEMS Microbiol. Ecol.* **52**, 185–195 (2005).
35. Froelich, P. et al. Early oxidation of organic matter in pelagic sediments of the eastern equatorial Atlantic: suboxic diagenesis. *Geochim. Cosmochim. Acta* **43**, 1075–1090 (1979).
36. Gaillard, J. F., Pauwels, H. & Michard, G. Chemical diagenesis in coastal marine sediments. *Oceanolog. Acta* **12**, 175–187 (1989).
37. Madison, A. S., Tebo, B. M., Mucci, A., Sundby, B. & Luther, G. W. Abundant Porewater Mn(III) is a major component of the sedimentary redox system. *Science* **341**, 875–878 (2013).
38. Postma, D. & Jakobsen, R. Redox zonation: equilibrium constraints on the Fe(III)/SO4-reduction interface. *Geochim. Cosmochim. Acta* **60**, 3169–3175 (1996).
39. Bethke, C. M., Sanford, R. A., Kirk, M. F., Jin, Q. & Flynn, T. M. The thermodynamic ladder in geomicrobiology. *Am. J. Sci.* **311**, 183–210 (2011).
40. Beckler, J. S., Jones, M. E. & Taillefert, M. The origin, composition, and reactivity of dissolved iron(III) complexes in coastal organic- and iron-rich sediments. *Geochim. Cosmochim. Acta* **152**, 72–88 (2015).
41. Oldham, V. E. et al. The speciation and mobility of mn and fe in estuarine sediments. *Aquat. Geochem.* **25**, 3–26 (2019).
42. Wu, F., Wan, G., Huang, R., Pu, Y. & Cai, Y. Geochemical processes of iron and manganese in a seasonally stratified lake affected by coal-mining drainage in China. *Limnology* **2**, 55–62 (2001).
43. Lovley, D. R. & Phillips, E. J. P. Manganese inhibition of microbial iron reduction in anaerobic sediments. *Geomicrobiol. J.* **6**, 145–155 (1988).
44. Zhao, Y. *The distribution and micro-biogeochemical behavior of sulfur speciation in sediment from plateau lakes: as exemplified by Erhai Lake Yunnan and Aha Lake Guizhou province, China*. M.S. thesis, University of Chinese Academy of Sciences, China (2006).
45. Wang, Y., Liang, X., Yuan, X., Zhang, W. & Zeng, J. Analyses of the vertical and temporal distribution of sulfate-reducing bacteria in Lake Aha (China). *Environ. Geol.* **54**, 1–6 (2008).
46. Jacobs, L. & Emerson, S. Trace metal solubility in an anoxic fjord. *Earth Planet. Sci. Lett.* **60**, 237–252 (1982).
47. Arakaki, T. & Morse, J. W. Coprecipitation and adsorption of Mn(II) with mackinawite (FeS) under conditions similar to those found in anoxic sediments. *Geochim. Cosmochim. Acta* **57**, 9–14 (1993).
48. Morse, J. W. & Luther, G. W. Chemical influences on trace metal-sulfide interactions in anoxic sediments. *Geochim. Cosmochim. Acta* **63**, 3373–3378 (1999).
49. Jin, Q., Roden, E. E. & Giska, J. R. Geomicrobial kinetics: extrapolating laboratory studies to natural environments. *Geomicrobiol. J.* **30**, 173–185 (2013).
50. Faivre, D. & Zuddas, P. Mineralogical and isotopic properties of biogenic nanocrystalline magnetites. in *Magnetoreception and Magnetosomes in Bacteria* (ed. Schüler, D.) 175–196 (Springer, 2007).
51. Buchachenko, A. L. Magnetic isotope effect: nuclear spin control of chemical reactions. *J. Phys. Chem. A* **105**, 9995–10011 (2001).
52. Beard, B. L. et al. Application of Fe isotopes to tracing the geochemical and biological cycling of Fe. *Chem. Geol.* **195**, 87–117 (2003).
53. Busigny, V. et al. Iron isotopes in an Archean ocean analogue. *Geochim. Cosmochim. Acta* **133**, 443–462 (2014).
54. Percak-Dennett, E. M. Iron isotope geochemistry of biogenic magnetite-bearing sediments from the Bay of Vidy, Lake Geneva. *Chem. Geol*. **360-361**, 32–40 (2013).
55. Rouxel, O., Sholkovitz, E., Charette, M. & Edwards, K. J. Iron isotope fractionation in subterranean estuaries. *Geochim. Cosmochim. Acta* **72**, 3413–3430 (2008).
56. Severmann, S., Johnson, C. M., Beard, B. L. & McManus, J. The effect of early diagenesis on the Fe isotope compositions of porewaters and authigenic minerals in continental margin sediments. *Geochim. Cosmochim. Acta* **70**, 2006–2022 (2006).
57. Tangalos, G. E. et al. Microbial production of isotopically light iron(II) in a modern chemically precipitated sediment and implications for isotopic variations in ancient rocks: microbial production of isotopically light iron(II). *Geobiology* **8**, 197–208 (2010).

58. Huerta-Diaz, M. A. & Morse, J. W. A quantitative method for determination of trace metal concentrations in sedimentary pyrite. *Mar. Chem.* **29**, 119–144 (1990).
59. Li, J. et al. Basaltic and solution reference materials for iron, copper and zinc isotope measurements. *Geostand. Geoanal. Res.* **43**, 163–175 (2019).

Acknowledgements

We thank Guilin Han for sharing the clean laboratory in the Surficial Environment Geochemistry Laboratory of China University of Geosciences (Beijing), R. Bastian Georg (Trent University) and Lu Yang (Beijing Createch Testing Technology Co., Ltd) for technical support in MC-ICP-MS analyses, and Shunda Yuan for helpful discussions. This paper is dedicated to the memory of Professor Yanguo Teng. This work was supported by the Natural Science Foundation of China (No. 42173006, 42377264) (L.S.) and National Natural Science Foundation of China (W2441015) (H.B.).

Author contributions

Conceptualization: L.S. and H.B.; Data acquisition: L.S., F.P., P.D., S.X., X.Z., Y.S., and Z.W.; Funding acquisition: L.S. and H.B.; Investigation: L.S., H.B., F.P., P.D., S.X., X.Z., Y.S., and Z.W.; Methodology: L.S., F.P., P.D., S.X., X.Z., Y.S., and Z.W.; Project administration: L.S. Resources: L.S., C.L.; Visualization: L.S. and H.B. Writing – original draft: H.B., L.S., and A.M.

Competing interests

The authors declare no competing interests.

Additional information

Supplementary information The online version contains supplementary material available at https://doi.org/10.1038/s43247-025-02931-9.

Correspondence and requests for materials should be addressed to Liuting Song or Huiming Bao.

Peer review information *Communications Earth and Environment* thanks Ernest Chi Fru and the other, anonymous, reviewer(s) for their contribution to the peer review of this work. Primary Handling Editors: Somaparna Ghosh.